Egyptian Geophysical Society
EGS Journal, Vol. 21, No. 1, 21-37 (2023)

MAPPING OF HYDROTHERMAL ALTERATION ZONES AROUND WADI ZUBEIR, NORTHERN EASTERN DESERT, EGYPT USING AIRBORNE GAMMA-RAY SPECTROMETRIC, AEROMAGNETIC AND REMOTE SENSING DATA

A.A. AZZAZY

Nuclear Materials Authority, P.O. Box 530, El Maadi, Cairo, Egypt.

رسم خرائط مناطق التغير الحراري المائي حول وادي زبير، شمال الصحراء الشرقية، مصر باستخدام البيانات الإشعاعية الطيفية الجوية لأشعة جاما والبيانات المغناطيسية الجوية وبيانات الاستشعار عن بعد

الخلاصة: يهدف البحث بصفة أساسية إلى استخدام البيانات الإشعاعية الطيفية الجوية لآشعة جاما والبيانات المغناطيسية الجوية وبيانات الإستشعار عن بعد لاستنتاج اماكن التمعدنات الموجودة فى منطقة وادى زبير وعلاقتها بالتراكيب السطحية والتحت سطحية. استخدمت البيانات الإشعاعية فى التعرف على أماكن تمركزات العناصر المشعة بمنطقة الدراسة متمثلة فى البوتاسيوم والثوريوم واليورانيوم. بالإضافة إلى ذلك تم استخدام البيانات الإشعاعية فى التعرف على اماكن التحلل باستخدام نسبة البوتاسيوم إلى الثوريوم. تم تحليل البيانات المغناطيسية المحمولة جواً باستخدام كاشفات الحواف (المشتقة الأفقية الكلية، الإشارة التحليلية، مشتقة زاوية الميل) للكشف عن اتجاهات البنية الجيولوجية المؤثرة على منطقة الدراسة. ساعدت أيضا بيانات الإستشعار عن بعد فى تحديد اماكن التحلل باستخدام تقنية نسبة النطاق (Band Ratio). يوضح التكامل بين خريطة نسبة K/eTh (البيانات الإشعاعية) وخريطة التغيير (Landsat 8 Band Ratio 6/7, 6/5, 5 in RGB) أن المناطق الرئيسية لمناطق التغيير ترتبط بشكل جيد وأساسي بالصخور الجرانيتية في شرق منطقة الدراسة. تُظهر خرائط الكثافة للتراكيب أن مناطق التمعدن لا يتم التحكم فيها فقط من خلال التركيب الصخري ولكن أيضًا من خلال التراكيب الموجودة بشكل رئيسي في اتجاه شمال غرب–جنوب شرق وإتجاه شمال شمال غرب–جنوب جنوب شرق.

ABSTRACT: *Airborne geophysical and satellite imagery were used to map hydrothermal alteration zones by analyzing the acquired data to provide accurate and reliable results. In the area around Wadi Zubeir, located in northern Eastern Desert of Egypt, airborne magnetic and spectrometric data, also satellite data were used to map hydrothermal alteration zones. The airborne radiometric data processed and gridded to generate the concentration maps of Potassium (K in %), Uranium (eU in ppm), Thorium (eTh in ppm) and ratios of K/eTh were computed to map the distribution of radioactive elements. The delineated geology and hydrothermally altered zones led to the identification of altered minerals. The altered zones were noted to be associated with mineralization in the granitic rocks. The delineated structures aided the design of the geologic map of the study area. The aeromagnetic data analyses performed to improve the quality of data for better understanding of the subsurface geology were reduction to the pole, total horizontal derivative, analytical signal, and tilt derivative. There are two main hydrothermal alteration zones have been identified. They show a spatial correlation with surface prospects and mineral occurrences, granite rocks, and main trends. Mapping of hydrothermal alteration zones associated with mineralization is of paramount importance in searching for metal deposits.*

1. INTRODUCTION

The study area is located in the northern part of Eastern Desert of Egypt, between Latitudes 27°25' 39" & 28° 07' 54" N and Longitudes 32° 16' 43" & 33° 10' 13" E and covers a surface area of about 4183 km^2 (Fig. 1a). The area is characterized by a high topography at the east with heights of about 1600 m and gradually decrease to the center of the area where the low valleys are encountered. Another high topography is found at the western and northern parts of the area. There are many mountains like G.Riseis, G.Ghuweirib G.Dara, G. Naqa, G. El Urf and G.Kifri and many wadis like wadi Umm Balad, wadi El Borga and wadi Zubeir. (Fig.1b).

The primary use of airborne gamma-ray surveys was in the exploration for uranium, with secondary uses for coal, lignite, radioactive heavy metal, and phosphate exploration (IAEA, 1979). In addition, data from airborne gamma-ray surveys have proved useful for detecting and mapping radioelement haloes around hydrothermal mineral deposits, especially the distribution of potassium alteration, and in differentiating between felsic (more radioactive) and mafic igneous rocks (Hoover et al, 1992). These capabilities may have applications in the tracing of known sources of crushed stone based on their radioactivity and in helping to identify surficial deposits derived from different sources, which may have implications for deposit quality estimates.

Airborne magnetic surveys are not normally flown for the purpose of mapping surficial deposits, although placer magnetite deposits can be found using airborne data (Hoover et al, 1992). To the contrary, airborne magnetic measurements are primarily used to detect and map the distribution of bedrock lithologies based on their magnetic properties. For example, aeromagnetic maps are a powerful tool for mapping the subsurface extent of exposed plutons and finding buried plutons (Elhusseiny, 2023). This capability may have application in the identification and mapping of bedrock suitable as a source of crushed stone or as a method for

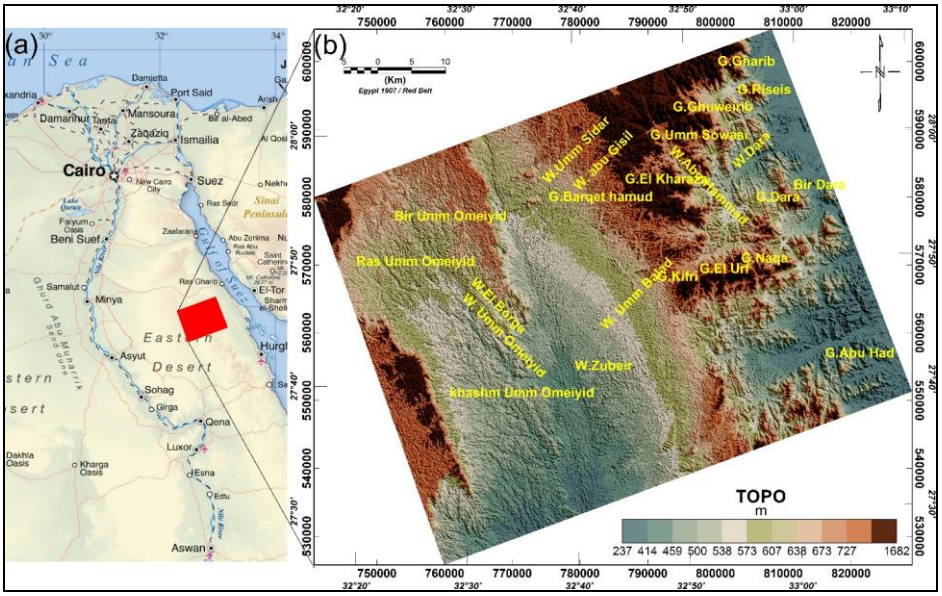

Fig. 1: (a) Location map of the study area, (b) Topographic map of the study area.

tracing the extent of a known source beneath surficial cover and overburden.

Remote sensing instruments measure reflected or emitted radiation in the visible, near-infrared, thermal infrared, or microwave portions of the electromagnetic spectrum to obtain information about the earth's surface from a distance. The information derived from remote sensing observations consists of two types: (1) information dependent on the physical properties (composition) of the surface materials (spectral reflectance, thermal emissivity, dielectric constant, etc.) and (2) indirect spatial information about the surface configuration (landforms, geologic structures, distribution of surface materials, etc.) (Kairu, 1982).

2. GEOLOGIC SETTING

The Eastern Desert is characterized as mostly occupied by a complex association of metasediments, metavolcanic, metagabbro, younger granites, older granites, and gabbroic rocks. This consequence is unconformably overlain by unmetamorphosed intermediate to silicic volcanic (Dokhan volcanic) and molasse facies clastic sediments (Hammamat clastics). The whole pile is intruded by a vast array of granite intrusions ranging in composition from quartz diorite to alkali- feldspar granite. Based on the geological maps of Egypt, at a scale of 1:500000 (Conoco, 1987), the area is part of the Northern Eastern Desert of Egypt. The Eastern Desert of Egypt is separated into northern, central, and southern parts based on basement characteristics and the structure features. Geology of the study area comprises a wide diversity of igneous, metamorphic, and sedimentary rocks ranging in age from Precambrian to Quaternary (Fig.2).

Sedimentary rocks overlie the Precambrian basement rocks unconformably and comprises several formations. The Precambrian rocks located at the northern and eastern parts mainly older granites calk-alkaline or grey granites at east to south part and younger granites or pink granites which weakly deformed at the northern part. Metavolcanics, metasediments and Hammamat sediment are located at northern and eastern parts separated by many wadies like Wadi Abu Hammad and wadi Dara. Dokhan volcanics are represented by calc-alkaline andesitic to rhyolitic rocks (Essawy and Abu Zeid, 1972). Metagabbro to meta diorite and their intrusive rocks are located at eastern and southern parts. Sedimentary rocks are located at the west and central area with Tertiary, Cretaceous and Quaternary. Tertiary represented by Thebes Formation with thinly bedded outer shelf chalk and chalky limestone rich in chert bands. Also Esna Formation formed of marine shale, calcareous intercalations. Cretaceous is represented by Galala Formation, umm Omeiyid Formation, Hawashiya, wadi Qena, Rakhiyat and Qusier and Duwi formations. Quaternary sediments are the youngest sediments recorded in the area that consist of pebbles of sand, detritus, fanglomerate, cobbles and little boulders filling the main wadis (Said, 1962). These originated as a result through the weathering process of the different types of the Red Sea Mountains.

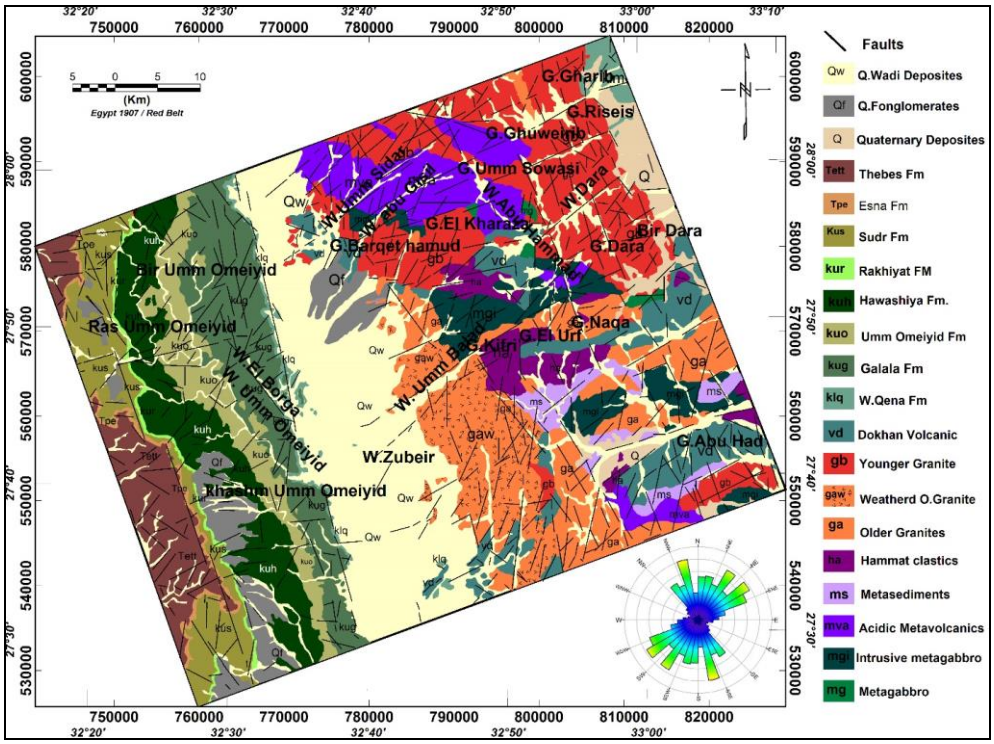

Fig. 2: Geologic map of the study area, after conco, 1987.

Several wadis are filled with Quaternary deposits (Fig. 2). The area is characterized by many faults with NW strike and small displacements that are now concealed by Quaternary alluvium. In addition, the area forms part of the African shield and is underlain by rocks ranging in age from Precambrian to Quaternary.

There are faults, fractures and shear zones as main structural features including thrust faults trending NW–SE direction (Gulf of Suez or Red Sea trend), NE-SW fractures which correlate Gulf of Aqaba trends. According to the rose diagram constructed from the geological map modified after Conoco (1987), figure (2) indicates that the area has main tectonic trends that are oriented along NE-SW, NW-SE, NNE-SSW, and NNW-SSE with minor traces of E-W trend. The area is extremely fractured and still affected by tectonic reactivation of the Red Sea, (Moustafa and Fouda, 1988).

3. DATA AND METHODS

Airborne gamma-ray spectrometry (AGRS), airborne magnetic and remote sensing data have been used to map the hydrothermal alteration zones associated with mineralization. The magnetic and spectrometry data were acquired along flight lines extending in NE-SW direction with 1.5 km spacing, while the tie lines were flown along profiles perpendicular to the flight lines (NW-SE) with 10 km spacing. The nominal flying altitude was 120 m above ground level (Aeroservice, 1984). Several image processing approaches that proved high accuracy for identifying the lithological units and detecting the alteration zones related mineralization.

4. GAMMA-RAY SPECTROMETRIC DATA

The gamma-ray spectrometry method is used in different fields. Initially developed as uranium exploration tool, the application of the method now includes geological mapping (Graham and Bonham-carter 1993; Charbonneau et al. 1997), mineral exploration (Lo and Pitcher 1996; Grasty and Shives 1997), soil mapping (Cook et al. 1996; Wilford et al. 1997), and environmental radiation monitoring (Sanderson et al. 1995; Ford et al. 2001).

Gamma-ray images are usually expressed as percent K and parts per million for eTh and eU. Images can be contrast stretched or ratio (eg. K/eTh) to highlight subtle variations in the data. Before images are generated from the flight line profiles, several corrections are applied to the data (eg. to remove noise). These corrections are not discussed here but are described at length by Minty (1997).

Geosoft (Oasis Montaj, version 8.4) software is used for gridding the dataset of K (%), eTh (ppm) and eU (ppm) and for the production of their respective grids, maps, ratio maps and the ternary images. The gridded images were used to interpret and map the geology of the area, making inferences to delineate high and low radiation anomalies related to the geology at various locations within the area. The generated radiometric maps of three radioactive elements and ratio

map also enhanced the delineation and mapping of zones that are hydrothermally altered.

4.1. Results

The radioactive data of total count (TC), potassium (K%), equivalent thorium (eTh) and equivalent uranium (eU) (Figs. 3-6) are relatively higher in radiometric values at the eastern parts than the western parts of the area. The recorded radioactivity varies widely from one type of rock to the other and some extent between the units of the same rock type. In some cases, the gradients are high enough for delineating the contacts, but sometimes the radioactivity levels of rock units merge into one another, without distinct separations between the different rock types. However, it is possible to distinguish the lithological contacts from the overall changes in the level of radiation.

4.1.1. TC, K, eTh and eU Concentration Maps

Total count (TC) map (Fig. 3) generally ranges from 0.94 µR/h to 24.34 µR/h. The high level concentration that ranges from (10 to 24.34µR/h) is associated with Younger granite (gb) and older granites (ga). The moderate concentration level ranges from (2.7 to 5.7µR/h) is observed at the western and central parts and related to Rakhiyat Formation (kur), Umm Omeiyid Fm (kuo) and Hawashiya Fm at the west. Another moderate concentration is around W. Zubeir at the central part. The lowest concentration level ranges from (0.9 to less than 2µR/h) is associated with Tertiary deposits like Esna Fm (Tpe) and Thepes Fm (Tett) at the far west, also at Galala Fm (kug) and Qena Fm (klq) at the middle area.

Potassium (K) map (Fig. 4) shows that Tertiary deposits like Esna Fm (Tpe), Thepes Fm (Tett) and many formations of Cretaceous like Galala and Qena Fms have lowest concentration level (0.01–0.4 %). While Rakhiyat Formation(kur), Umm Omeiyid Fm (kuo), Hawashiya Fm (kuh) and Quaternary deposits have the moderately level (0.4–1.5%). Younger granites (gb), older granites (ga) Dokhan Volcanic (vd) and Hammamat sediments (ha) have the highest one (1.5–4.2%).

Equivelent thorium map (eTh) shows that the highest level reaches to 44.1 ppm associated with younger granite (gb), older granites (ga), and Dokhan Volcanic (vd) at the east. Intrusive metagabbro at the east and the Cretaceous rocks at the west represent the moderate level ranged from (2.9 to 5.9 ppm). The lowest concentration level in the eTh map (Fig.5) is related to Esna Fm (Tpe) and Thepes Fm (Tett) at the far west and also at Galala Fm (kug).

Equivalent uranium (eU) map (Fig.6) shows high radioactive values at younger granites and older granites reach to more than 12 ppm at the eastern part. The high values of uranium concentration at the west are associated with Sudr Formation and Rakhiyat Fm which is carbonate and phosphate beds. The moderate level is associated with Quaternary deposits all over the area Umm Omeiyid Fm (kuo) ranges from 1.6 to 2.5 ppm. Galala Fm (kug) and Qena Fm (klq) at the middle area are the lowest values range from 0.1 ppm to 1.6 ppm.

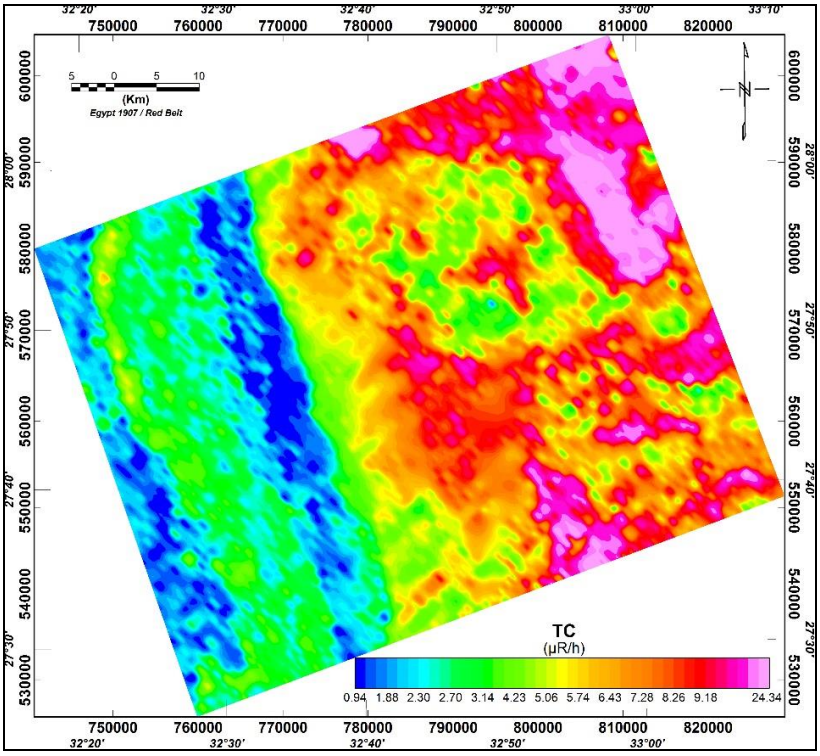

Fig. 3: Total count (TC) map of the study area.

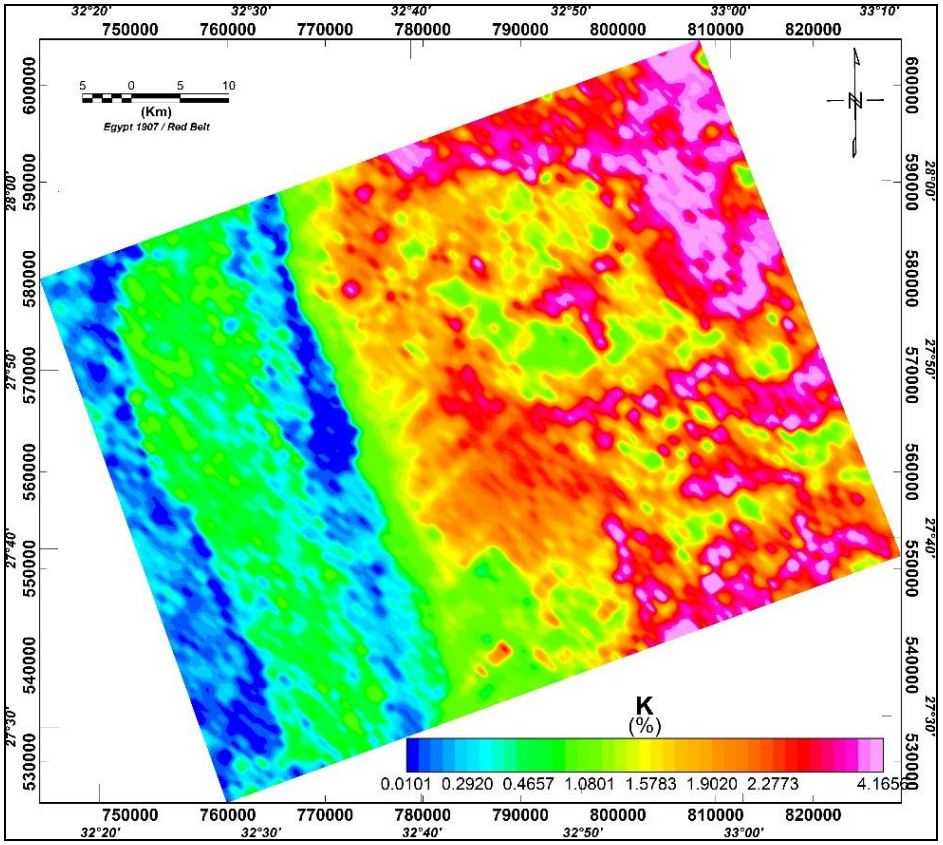

Fig. 4: Potassium (K) map of the study area.

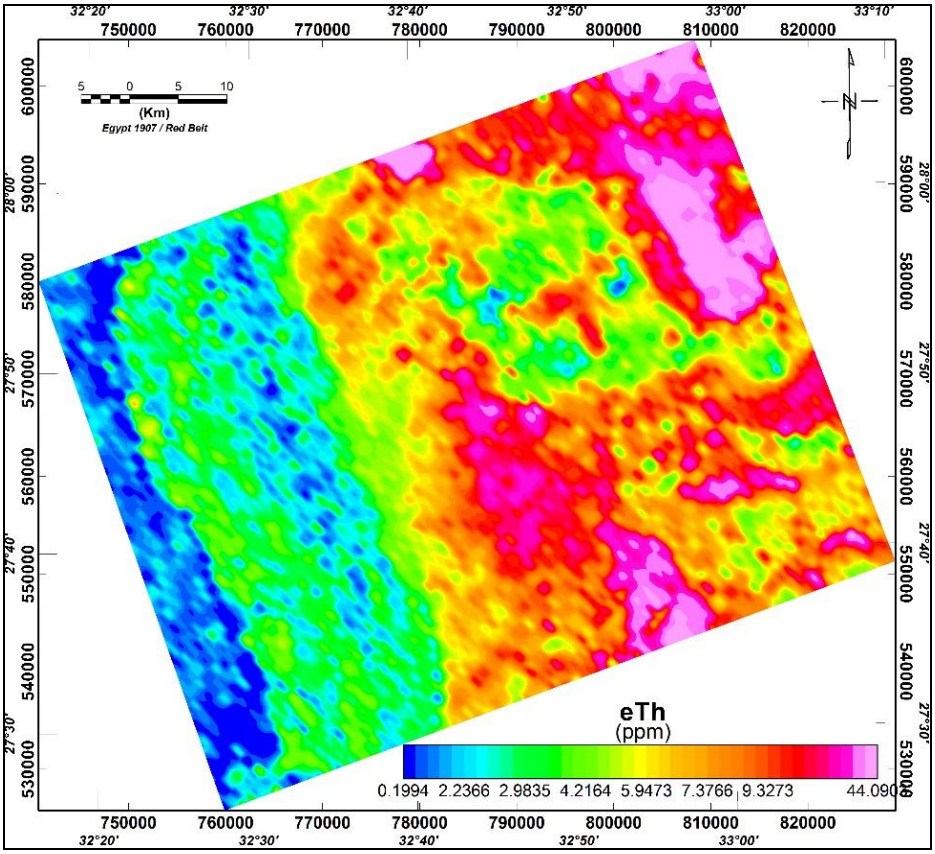

Fig. 5: Equivalent thorium (eTh) map of the study area.

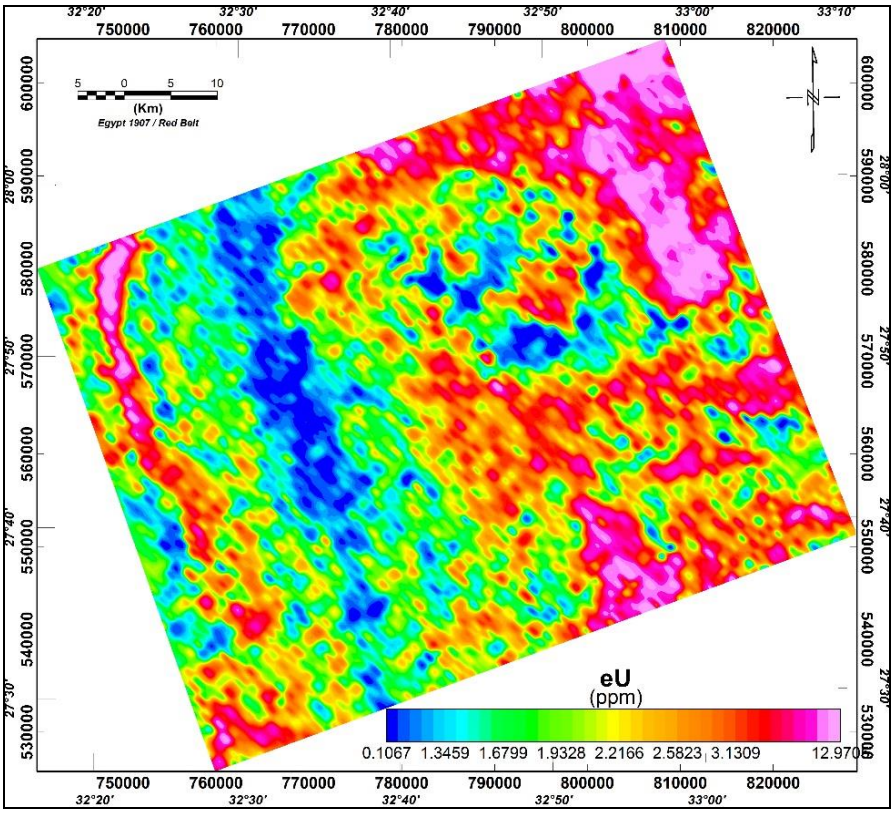

Fig. 6: Equivalent uranium (eU) map of the study area.

4.1.2. Mapping of Hydrothermal Alteration Zones

The concentration of potassium is a key factor in the identification of geologic rock units that are affected by hydrothermal systems favorable for the development of mineralization. Potassium is normally added to host rocks by mineralizing hydrothermal solutions; it is therefore the most reliable pathfinder in airborne gamma-ray surveys in locating hydrothermal ore deposits, especially gold deposits (Hoover and Pierce, 1990). Minerals such as K-feldspar and muscovite are normally the sources of K in rocks that are hydrothermally altered, and these minerals can be detected by a rise in K counts. Rocks that are free of these minerals have very low K-activity. Thus, K activity is very low in all mafic and ultramafic rocks (Ibe, S. O. & Nwokeabia, C. N., 2020). Potassium concentrations generally increased with increasing weathering processes (Takyi-Kyeremeh et al. 2019).

Weathering and metamorphism can modify the radioelement content of rocks profoundly (Ibe, S. O. & Nwokeabia, C. N., 2020). Uranium is easily oxidized to a water-soluble form; and can be readily leached from pegmatites and granites and redeposited in sediments at large distances from the source rock. Thorium has no soluble ion and therefore tends to remain with the parent rock or is transported over relatively short distances in the form of solid mineral grains. Common thorium-bearing minerals such as zircon and monazite are heavy and thus accumulate in placers and in the heavy mineral fraction of clastic sediments (Ibe, S.O. & Nwokeabia, C.N., 2020).

Hoover et al, 1992 showed that the Potassium/Thorium ratio is nearly constant in most rocks and generally ranges from 0.17 to 0.2 (K/eTh). Values of the k/eTh ratio that exceed this range could be due to hydrothermal alteration processes associated with the emplacement of magmatic-hydrothermal mineralization. K/eTh ratio was calculated to locate high values of potassium content (Fig. 7). High concentrations of this element may reveal possible areas of hydrothermal alteration and mineralization (Henaish, et al, 2022.). The K/eTh ratio is often considered the best indicator of potassium enrichment zones related to hydrothermal alteration.

Zone (A) presents extremely high K/eTh values reach 1.15, associated with alteration zones probably linked to mineralized zones. This zone located at east, north and southeast and associated with younger granites, intrusive metagabbro and metasediments (Fig.7). Zone (B) which has values of K/eTh ratios 0.2-0.3 at the east and are related to parts of intrusive metagabbrog and older granites, and at the center related to Quaternary wadi sediments at wadi Zubeir. However, there are high values of k/eTh alteration at the western part associated with parts of Galala Formation, Hawashiya Formation and Sudr Formation. These places of alteration and mineralization in sedimentary rocks, whether in the middle or west of the region, may be the mineralization of radioactive rocks, and they

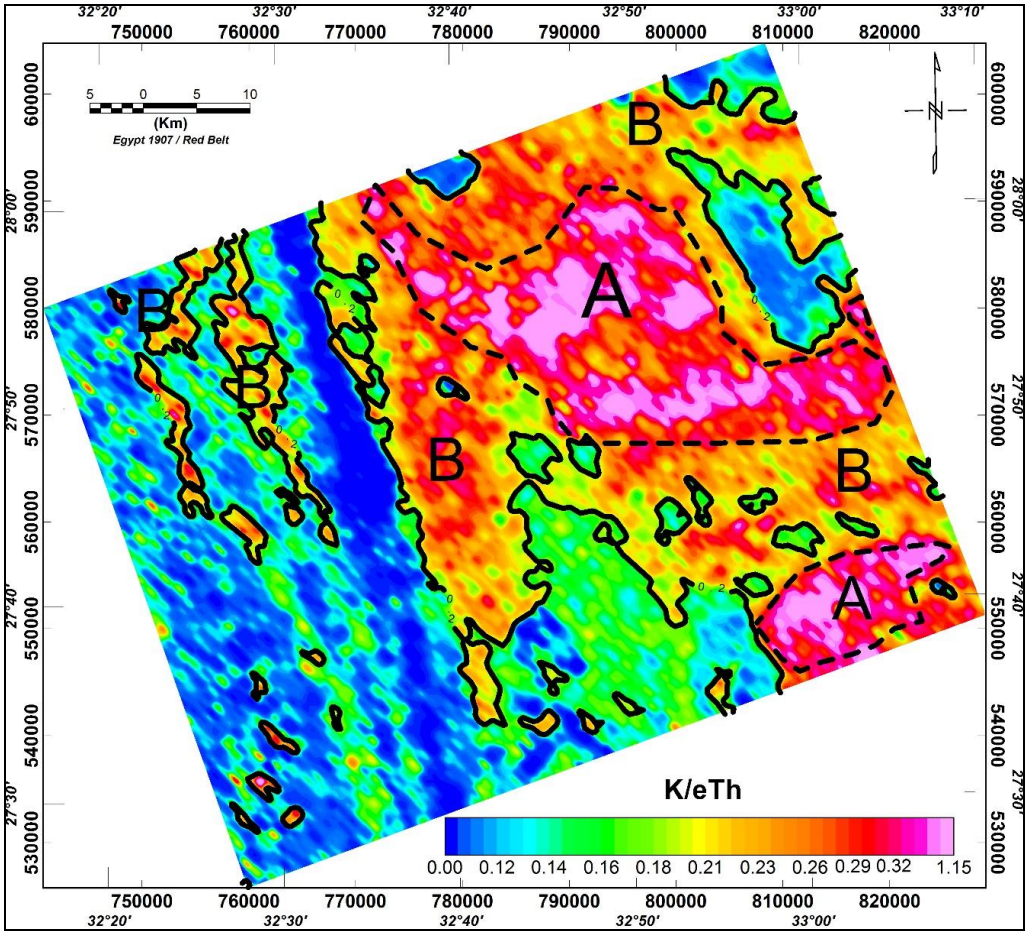

Fig. 7: Potassium/Equivalent thorium ratio (K/eTh) map of the study area.

were transferred as a result of the transmission of radioactive elements during migration. In general, areas with a K/eTh ratio greater than 0.2 are strong indicators of hydrothermal changes throughout the area. These zones of alteration are trending mainly NW- SE. The highest values are associated with igneous rocks such as younger granites.

5. AEROMAGNETIC DATA

To assist delineation of lineaments and create structural complexity maps, firstly, the total magnetic intensity map (Fig. 8) was reduced to the pole to locate the magnetic anomalies directly above their source bodies. The Aeromagnetic data which constructed by Aero-Services Company, 1984 aimed essentially at providing data that would assist in identifying and assessing the mineral, petroleum and groundwater resources of the region. The digitized aeromagnetic map was imported into the Geosoft Oasis Montaj software environment and then aeromagnetic data were reduced to the pole. Generally, for good accuracy in interpretation of the magnetic anomaly map, it has to differentiate the hypothetical anomaly from the observed type on the total intensity magnetic map, where the causative body can be directed to the northern pole. RTP (Reduction to the pole) of the total magnetic field application removes the asymmetric anomalies caused by the inclination and centering the anomalies directly above their broad deep-seated sources (Elhusseiny and Azzazy, 2021).

5.1. Results

5.1.1. Total Magnetic Intensity (TMI) Map

TMI map shows magnetic anomalies with magnitude values range from -595 nT to 404 nT. These anomalies can be grouped into high and low magnetic anomalies. The highest values are located at the southwestern, many locations at the east and at central related to W. Zubeir. These high magnetic anomalies may indicate a shallower basement and/or thin sedimentary cover. The southwestern positive anomalies may be related to the basic and ultrabasic roots of basement rock extended at high depth and appear at the southern part of the Eastern Desert. This configuration of positive anomalies may be attributed to relatively deep-seated low relief basement structures. This suggests that the TMI anomalies are strongly influenced by the regional tectonic. The high positive anomalies at the east of the area are relatively affected by metagabbro and its intrusive. The lowest values are located at the northeastern and northwestern parts, also many locations at the east at G. El Urf and G. Naqa (Fig. 8).

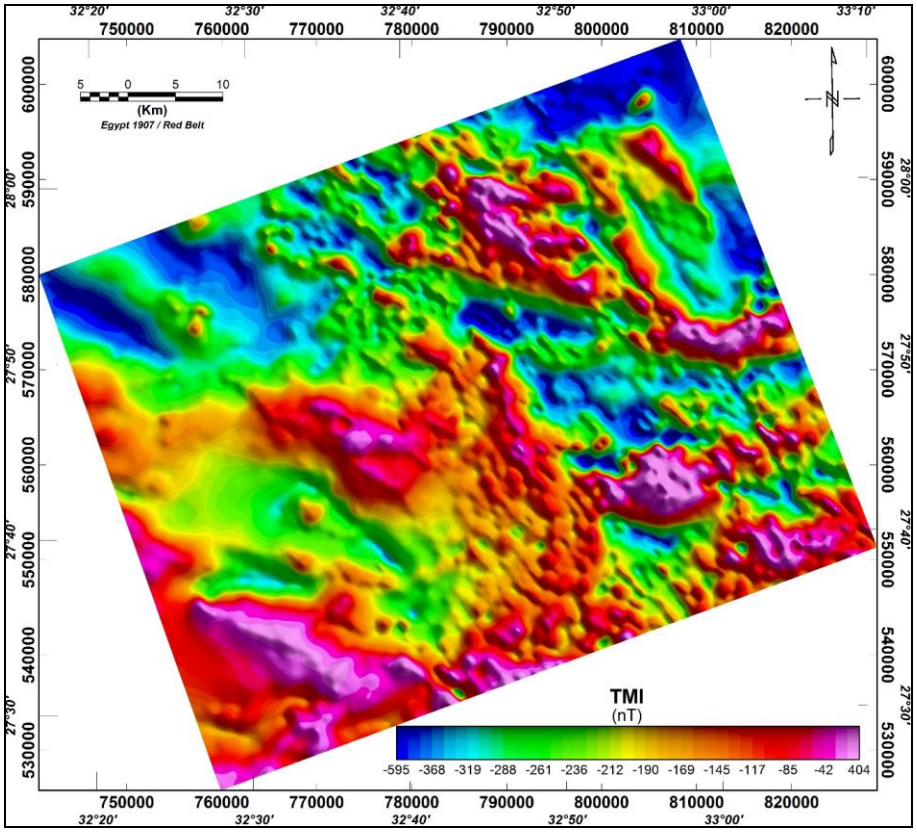

Fig. 8: Total magnetic intensity map of the study area.

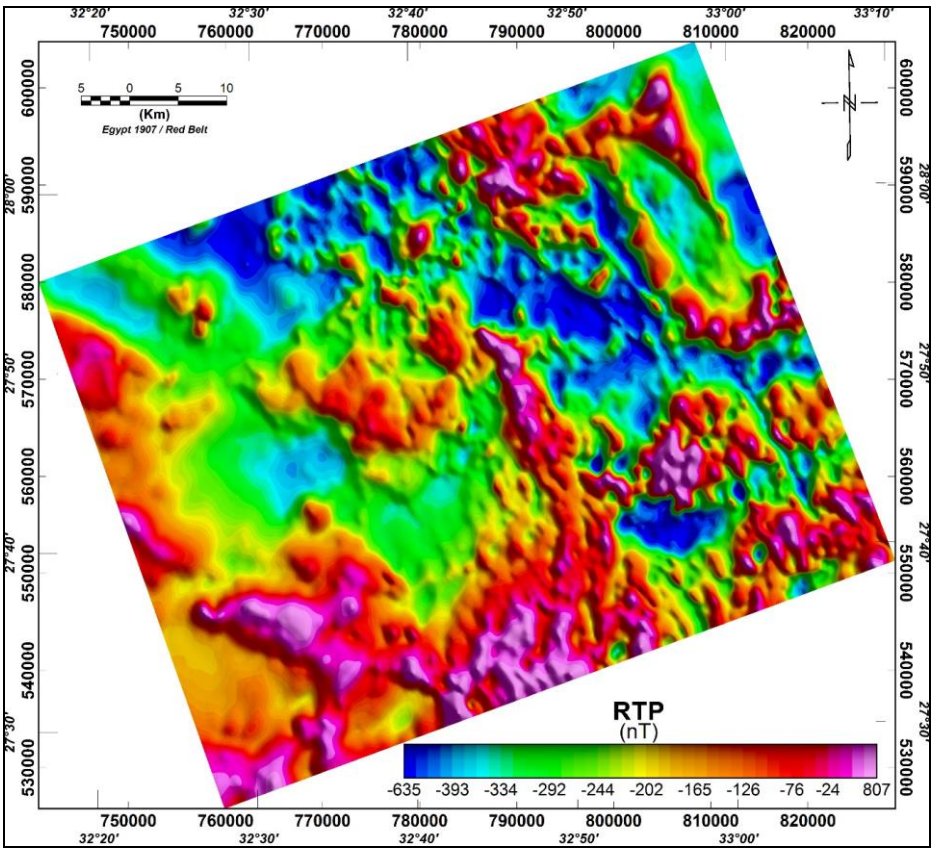

Fig. 9: Reduced to magnetic (RTP) map of the study area.

5.1.2. Reduced to the Pole Magnetic (RTP) Map

The position and shape of the obtained magnetic anomalies are then related to their subsurface source bodies in the area. The RTP map shows magnetic intensity values between -635 nT and 807 nT. The northeastern, western, southwestern, and southern parts of the map are characterized by the presence of high amplitude magnetic anomalies from -76 nT to 807 nT with elongated and semicircular shapes that may be due to shallow bodies of high magnetic. The northern and eastern parts of the study area are characterized by low magnetic amplitudes ranging from -639 nT to -334 nT whereas the central and some parts at the east are characterized by moderate magnetic amplitudes between -334 nT and -76 nT (Fig. 9).

The map of RTP magnetic map shows the observed magnetic anomalies directly over the magnetic source bodies and sharpens the contacts between the magnetic high and low patterns as well as anomalously high magnetic susceptible zones probably coming from deeper sources. The main trend for the RTP map is northwest-southeast that is affected by the tectonic movement at the Eastern Desert.

5.1.3. Analytic signal map (AS)

Analytic signal is a veritable tool for locating the edge of magnetized bodies. The analytic signal peaks and centers over magnetic source(s), among others, include lithological contacts, faults, fractures, shear zones and intrusive. Analytic signal map of the study area has amplitudes that range between 0.002 and 1.58 nT/m. High magnetic anomalies at analytic signal map are observed around G.Riseis, G.Ghuweirib G.Dara, G. Naqa, G. El Urf ,G.Kifri and G. Abu Had in the north-eastern, east and south-eastern parts of the area, showing amplitudes in the range of 0.17 to 1.58 nT/m (Fig. 10a). These truncated magnetic anomalies could reflect the imprints of deformation in the area and are seen to trend approximately in the NW–SE and WNW–ESE directions. The high expression of AS anomalies can be attributed to the presence of faulted porphyritic granite rocks. These magnetic anomalies are corresponding to geologic structures that can provide migration pathways for the plumbing of mineralizing fluids and localization of mineral deposits in the study area.

5.1.4. Tilt derivative (TD) map

Generally, TD map has a good correlation with local geology (fig. 2) trends as in the area; thereby it serves as an effective tool for a reliable structural mapping. Continuous, thin and curvilinear magnetic patterns that are characteristic of lithological contacts and major geological structures in the study area are better accentuated on the TD map (Fig. 10b). Similarly, magnetic anomalies on this map trend principally in the NW–SE direction, thus reflecting the footprints of the Pan-African orogeny in the area.

5.1.5. Total horizontal derivative (THD) map

Total horizontal derivative map (THD) reflects structural complexity of the basement rock in the study area (Fig. 10c). On the THD map, peak anomalies are often observed over geologic contact zones such as fracture, shear zones and faults (Sanusi and Amigun, 2020). The amplitudes of the total horizontal gradient range between 0.0002 and 1.098 nT/m. The area can be demarcated into two main fractured zones eastern and western parts.

As a result of high magnetic susceptibility contrast between the adjacent magnetized blocks, the eastern zone shows peaks of high gradient anomalies that correspond to geological contacts like lithological contacts and fractures. The main trends at the eastern zone are NW–SE, NNW–SSE and ENE–WSW. The western zone is marked by weakly magnetized bodies that trend NW–SE. The amplitudes of the THD in this zone vary between 0.0002 and 0.045 nT/m, which are typical of low magnetic susceptibility bodies (Fig. 10c).

According to resulted lineation maps, the NW-SE and NNW-SSE direction is the predominance trends in the study area whereas NE-SW trend appeared in geologic structure lineaments (Fig. 2).

6. REMOTE SENSING DATA

Band ratio is a multispectral image processing method that includes the division of one spectral band by another. Various bands of Landsat 8 satellite imagery used for band ratio which related to airborne radioactive changes. (Azzazy, et al, 2022).

Remote sensing data used to identify areas of hydrothermal alterations and extracting the surface lineaments that affect the study area. The bands 7, 5, 3 in R, G, and B used to present composite image to distinguish between felsic, mafic and wadi deposits. Generally, the basement rocks at the east appeared as dark colors, composite image shows that felsic rocks appear in reddish brown color, the mafic rocks are dark; however, the bright colors at the middle and western parts according to the presence of wadi deposits and sedimentary rocks (Fig. 11). Also, Landsat composite image shows good correlation with geologic map and its lithology content.

Mineralization produced using band ratio to improve the spectral characteristics of the alteration regions depending on the absorption bands of their altered minerals. For example, using Landsat-7 the iron bearing (ferrous and ferric oxides) minerals are delineated using band ratios 3/5 and 5/4 (Sultan et al., 1986) and 3/1(Abrams et al., 1983). Moreover, band ratio 5/7 was applied to detect high values of the hydroxyl-bearing minerals (kaolinite, alunite, muscovite, epidotes and chlorites) (e.g., Gupta, 2003).

The areas of hydrothermal change are clearly marked in a bright tone by applying the 6/7 band ratio of the Landsat-8 OLI (Fig. 12). Alteration changes in the east is associated with granite rocks and some metamorphic rocks.

Using band ratio composites 6/7, 6/5, 5 in R, G, and B, (Ramadan et al., 2001; Ramadan and Sultan, 2004) highlight the alteration areas that clearly marked in yellow color (Fig. 13).

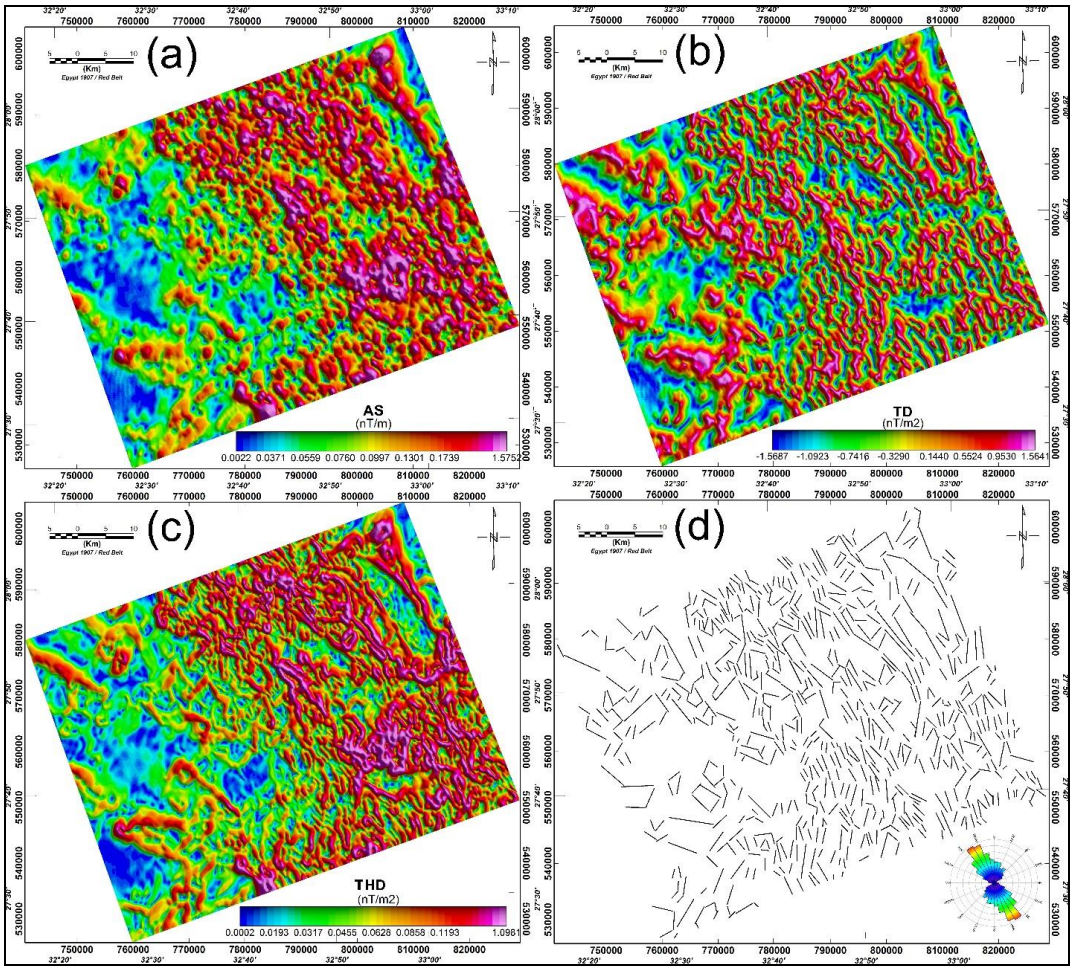

Fig. 10: (a) Analytic signal, (b) Tilt derivative, (c) Total horizontal derivative of RTP data, and (d) the resulted lineation and its rose diagram.

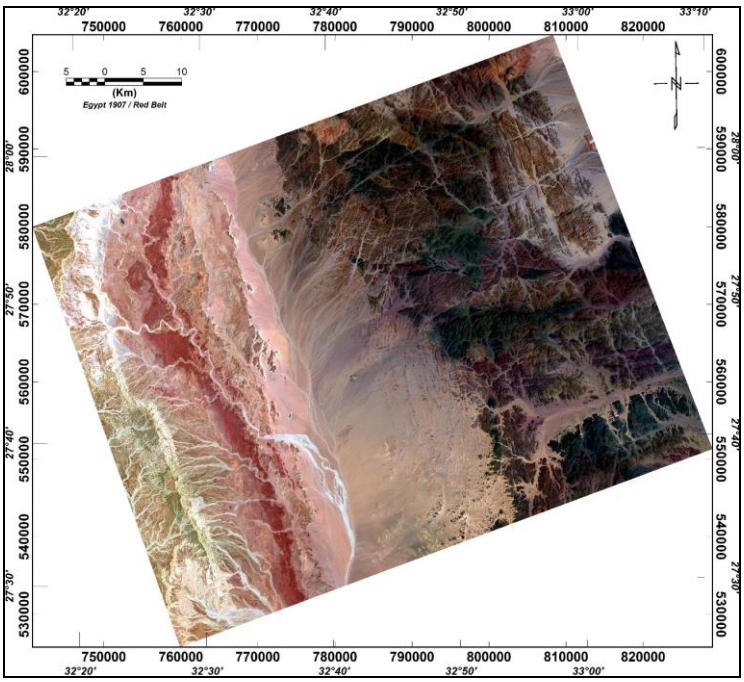

Fig. 11: Landsat-8 composite image 7, 5, 3 in R, G, and B.

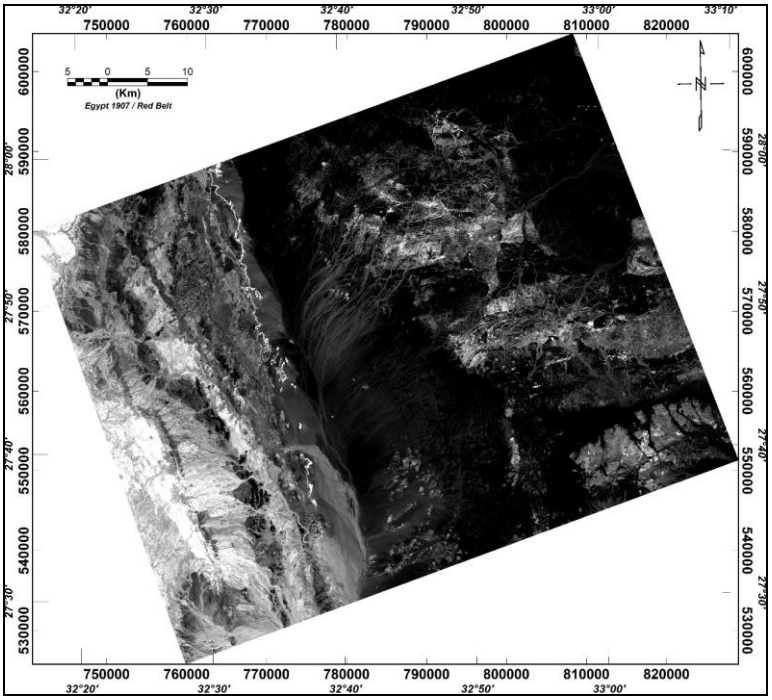

Figure 12: Alteration 6/7 band ratio of the Landsat-8.

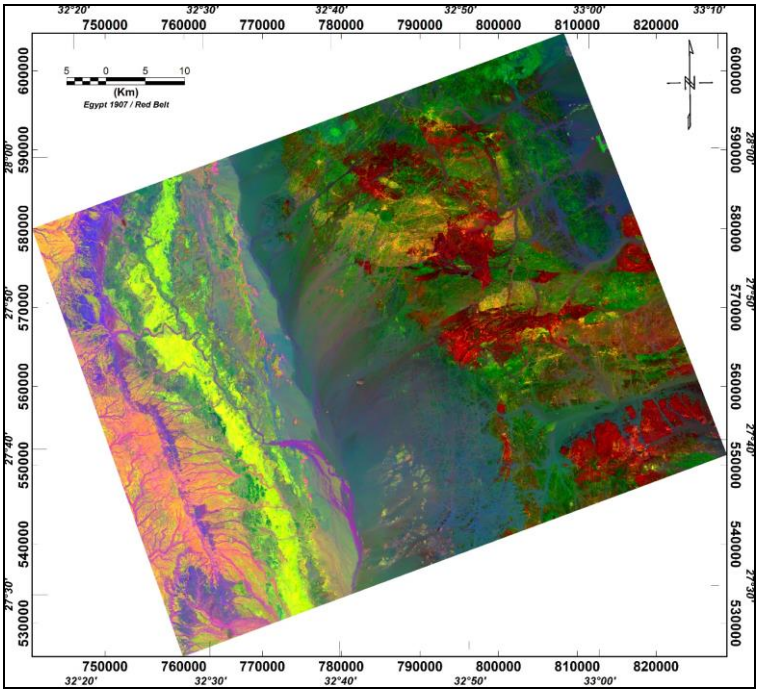

Fig. 13: 6/7, 6/5, 5 in R, G, and B composite image reveals the alteration areas.

Band ratio 5/4 was used for detecting the alteration zone of ferrous and ferric minerals and iron oxide alteration (hematite, goethite and jarosite) in the study area as shown in figure (14) in which these alteration areas are represented by the white color surrounded by the grey color. For detecting the alteration zone of the hydroxyl (OH)-bearing minerals, the band ratio 5/7 is used, as shown in figure (15). The high abundance of all these mapped minerals is typically associated with Dokhan volcanics, Hammamat sediments and some parts of the granitic rocks. It shows a strong correlation with the mineral occurrences and prospects in the study area. This band ratio displayed the OH-bearing menials (5/7 ratio) in R, the Fe-bearing menials (5/4 ratio) in B and OH + Fe (5/7 + 5/4) in G (Fig. 16), which appear in very light pink colour at the eastern part which is mainly related to younger granites. High favorability index values are mapped in granites and volcanic rocks, also some parts at the west and middle of the area.

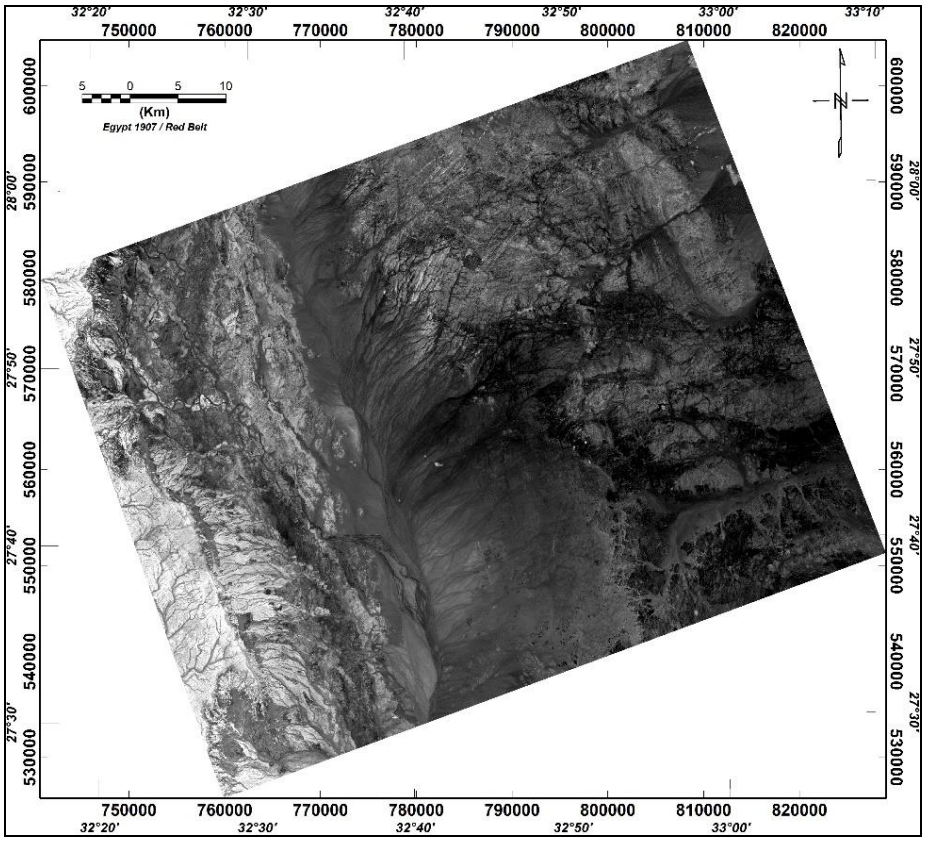

Fig. 14: Band ratio 5/4 of Landsat-8 (Fe- minerals)ز

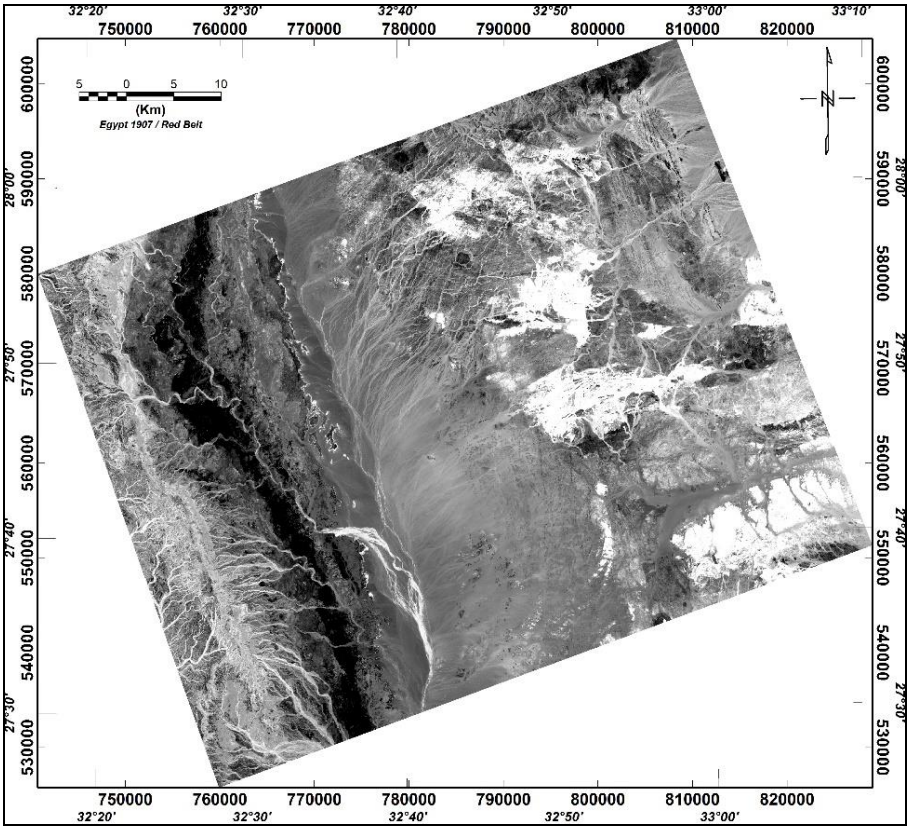

Fig. 15: Band ratio 5/7 of Landsat-8 (OH-bearing minerals).

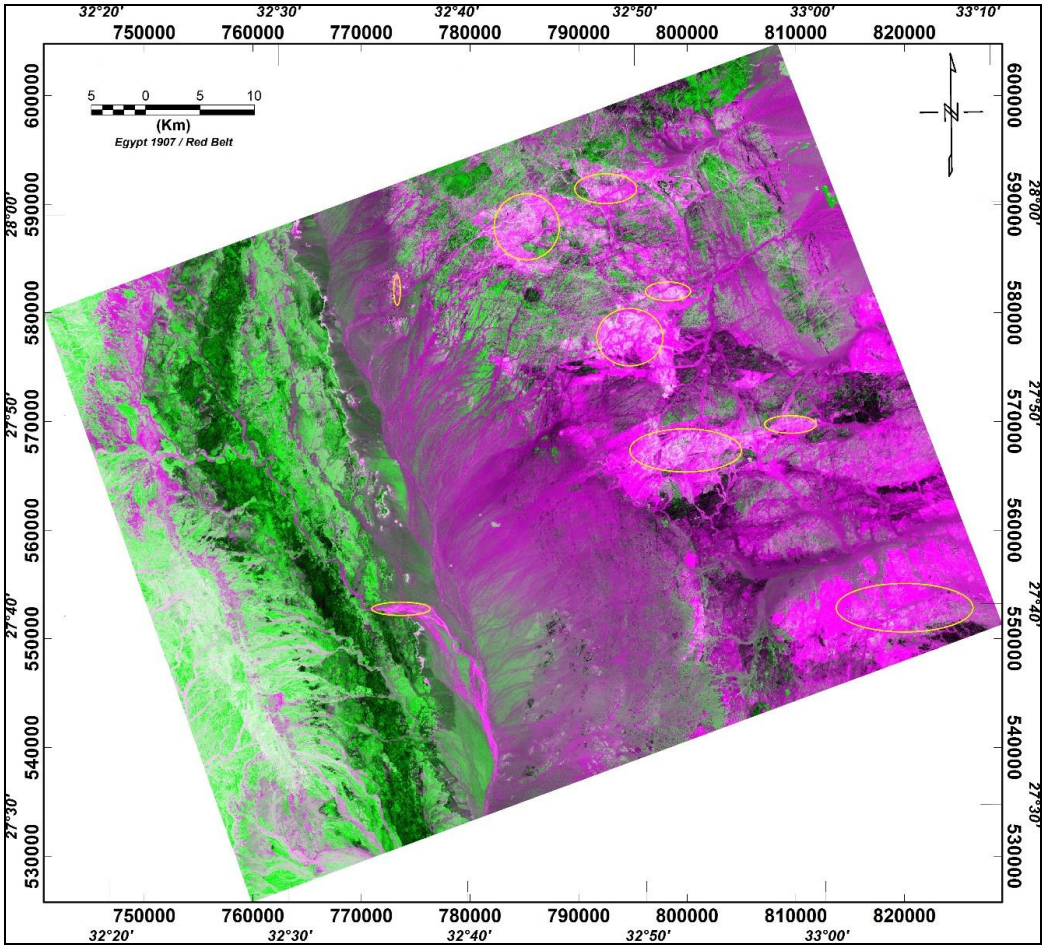

Fig. 16: Band ratio image showing the alteration areas of ore deposits mineralization represented with very light pink color after displaying OH in (R), Fe in (B) and OH+F in (G).

7. DISCUSSION AND RESULTS

7.1. Tectonic Affected Alteration Zones

For determining subsurface structure and basement configuration, magnetic data is used. subsurface structure trends (deep and shallow trends) were delineated through magnetic method by using the edge detectors (THD, AS and TD) and presented in figure (10).

In addition to subsurface structure trends deduced from magnetic method, surface Landsat-8 satellite data and their analyzed images are very effective for lineaments mapping (Marghany and Hashim, 2010; Mwaniki et al., 2015; Kamel et al., 2016). The Landsat-8 structure lineaments deduced by using automatic extraction using the LINE tool in PCI Geomatica 2013 software. This algorithm improves the data edges through specific parameters as edge detection, thresholding, and curve extraction (e.g.: Zoheir et al., 2019).

Density map technique was applied to the lineaments determined by satellite image and presented in figure (17), to determine the structure trends affecting the study area. The line density map was resulted using the ArcMap line density tool; presenting the frequency of lineaments per unit area.

The high density reflects the variation of surface structural of the exposed rock units, as we find that the different and frequent tectonic movements in this area are very impressive. The highest density is found in the east of the region, especially related to basement rocks which are highly deformed by many faults. Also, there are high density at the western part by structural tectonic movements.

The rose diagram (Fig. 17) show that NNW-SSE and NW-SE directions are the predominance trends in the study area. In addition, magnetic trends map (Fig. 10) show that the most effected trend is NW-SE and NNW-SSE directions whereas NE-SW trend appeared in geologic structure lineaments (Fig. 2).

7.2. Alteration Zones

The processing of the geophysical and remote sensing data used in the present work is very important step for recognizing new potential targets for mining research at the area. The combination of these different data types allowed us to map in detail the hydrothermal alteration zones associated with the metal deposits.

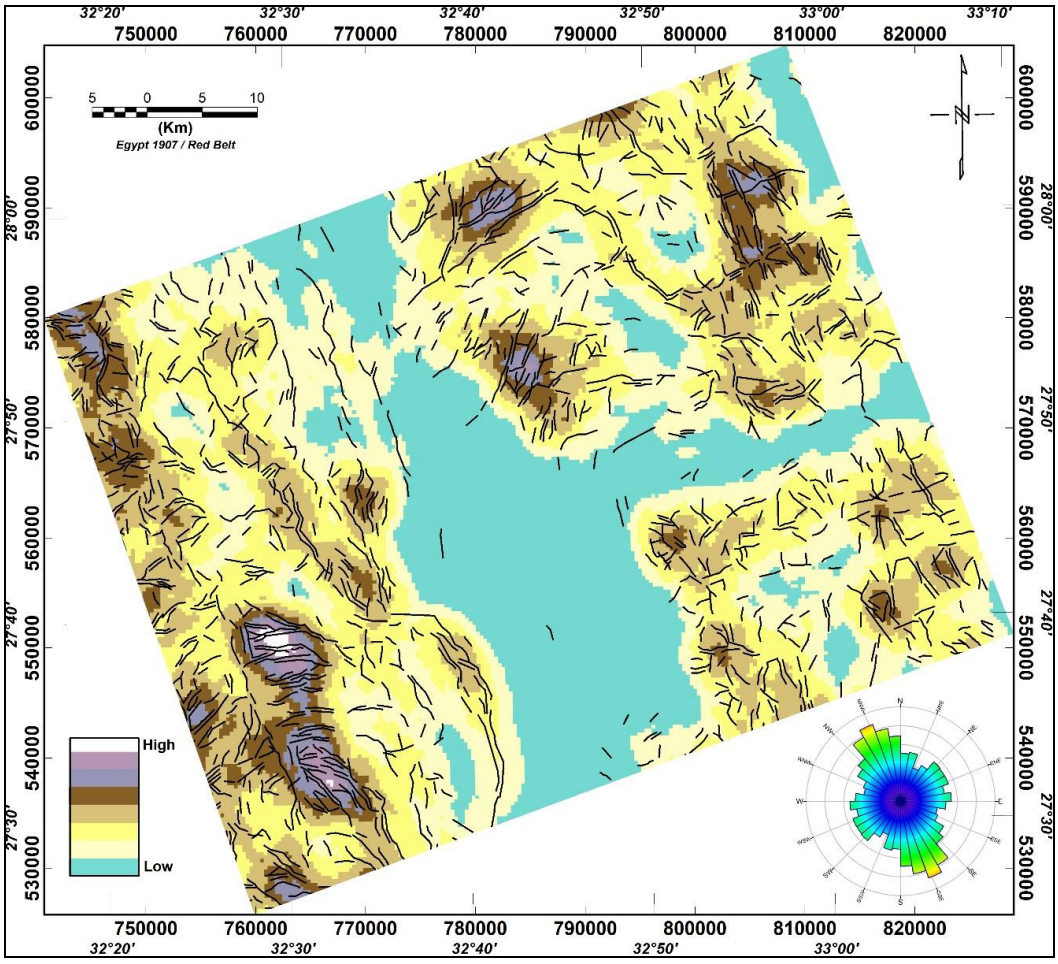

Fig. 17: Satellite image lineation on density lineaments map with its rose diagram.

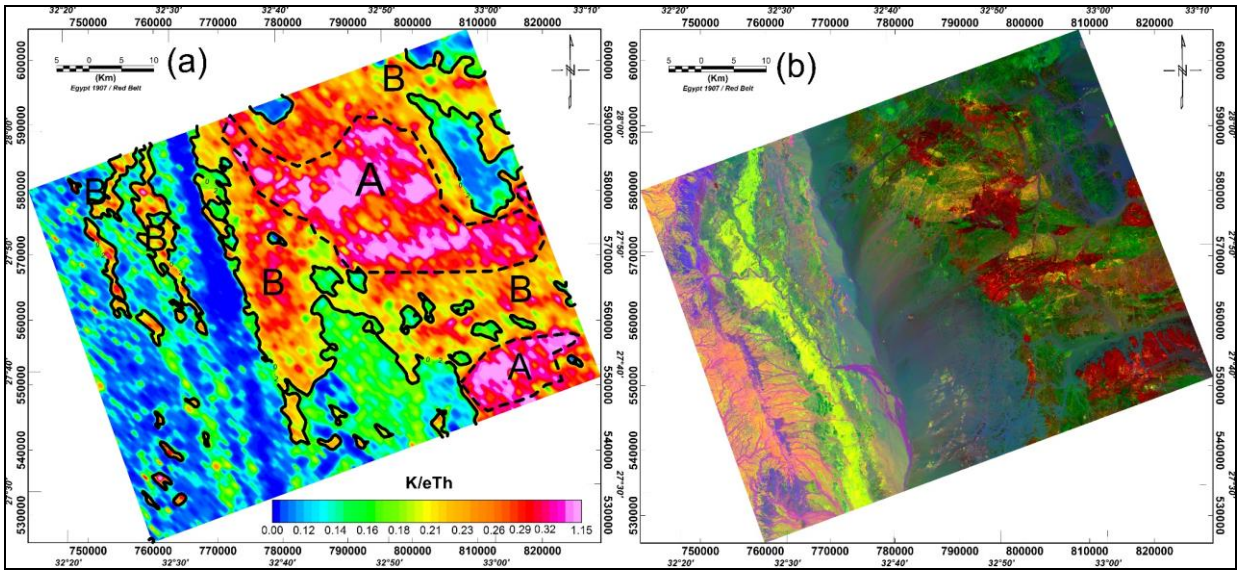

Fig. 18: Integration between (a) K/eTh ratio image, (b) Landsat composite image.

Hydrothermal altered zones are mapped from the K/eTh ratio map (Fig. 7). these zones affected by structure fractures, they serve as channel pathways for migrating Hydrothermal fluids that contemporaneously reacts with rock formation which got altered subsequently. The alteration zones marked by high density lineation and high potassium content that lie within or close to a structure that has NW and NNW trends identified previously. The confidence areas of these alteration zones and high complexity lineaments and porphyry indicated a high possibility for the occurrence of minerals in other similar locations.

The K/eTh ratio which calculated to highlight enrichment zones in this element showing two main alteration zones (Fig. 18), also satellite image shows probable locations that were marked yellow colors. Thus, as mentioned previously the tight concordance between these known mineralization locations and the interpreted structural complexities sheds a light towards the similar mapped features that may be new promising sites. However, precise detection and evaluation of these ores need more geological and geophysical follow up survey with finer spacing.

8. CONCLUSION

The integrated study helped in getting a better understanding of the geology and mineralogy of the area. The detailed mapping for the studied area indicated different magmatic activities associated with high-potential fluid phases. The high potential fluid phases altered and weakened the granite making it easily weathered developing the isolated and cavernous arc-shaped granitic masses of low to moderate relief. Geophysical data and satellite images revealed that the study area was affected by several tectonic events. These tectonics resulted in a highly-fractured and jointed granite representing a good open system permitting the solution to pass and leach, causing mineral redistribution and concentration. Airborne magnetic data were analyzed using edge detectors (THD, AS and TD) to detect the geologic structure trends affecting the study area. In addition, radio-spectrometry and Landsat image helped to determine alteration zones and mineralization. The integration between K/eTh ratio map (spectrometry data) and alteration map (Landsat 8 Band Ratio 6 / 7, 6 / 5, 5 in RGB) clarifies that the main areas of alteration zones are well correlated mainly to granitic rocks at the east. Structure Density maps show that mineralization zones are not controlled only by lithologic composition but also by structures mainly in NW-SE and NNW-SSE direction.

REFERENCES

Abrams, M.J., Brown, D., Lepley, L. and Sadowski, R. (1983): Remote Sensing for Porphyry Copper Deposits in Southern Arizona. Economic Geology, 78, 591-604.

Aero Service, (1984): Final report on airborne magnetic/radiation survey in Eastern Desert, Egypt. Work Completed for the Egyptian General Petroleum Corporation (EGPC). Six volumes, Aero Service, Houston, Texas, USA.

Azzazy, A. A, Elhusseiny, A.A and Zamzam, S., (2022): Integrated radioactive mineralization modeling using analytical hierarchy process for airborne radiometric and remote sensing data, East Wadi Qena (EWQ), Eastern Desert, Egypt, Journal of Applied Geophysics 0926-9851/© 2022 Published by Elsevier B.V.

Conoco, Inc., (1987): Geological Map of Egypt 1:500 000, Conoco Inc.

Cook, S.E., Corner, R.J., Groves, P.R., Grealish, G.J., (1996): Use of airborne gamma radiometric data for soil mapping. Aust. J. Soil Res., 34, 183-194.

Charbonneau, B.W., Holman, P.B., Hetu, R.J., Mac Queen, (1997): Airborne gamma spectrometer magnetic-VLF survey of northeastern Alberta, Exploring for Minerals in Alberta: Geological Survey of Canada Geoscience Contributions, Geological Survey of Canada Bulletin, vol. 500. Canada-Alberta Agreement on Mineral Development, pp.107–132.Core, D., Buck

Elhusseiny, A.A. and Azzazy, A.A. (2021): Depth and Structural Parameters Determination of the Sedimentary Basin in Atmur Nuqra Area, South Eastern Desert, Egypt Using Aero-magnetic

Elhusseiny, A.A. (2023): Integrated Structure and Mineralization Study Using Aero-Magnetic, Aero-Spectrometric and Remote Sensing Data at Esh El-Mallaha Area, Eastern Desert, Egypt. Geomaterials, 13, 1-22.

Essawy, M.A. and Abu Zeid, K.M., 1972: Atalla Felsite Intrusion and Its neighboring Flows and Tuffs, Eastern Desert, Ann. Geol. Surv. Egypt, 2, 271–280.

Ford, K.L., Savard, M., Dessau, J.-C. and Pellerin, E., (2001): The role of gamma-ray spectrometry in radon risk evaluation: A case history from Oka,Quebec. Geoscience Canada, 28, 2. Data Analysis. Geomaterials, 11, 23-41.

Graham, D.F., Bonham-carter, G.F., (1993): Airborne radiometric data: a tool for reconnaissance geological mapping using a

GIS, Photogrammetric Engineering and Remote Sensing, 58, 1243-1249.

Grasty, R.L.; Shives, R.B.K. (1997): Applications of gamma ray spectrometry to mineral exploration and geological mapping. In Proceedings of the Workshop Presented at Exploration, Houston, TX, USA, 4–5 October; Volume 97.

Gupta, R.P. (2003): Remote Sensing Geology. 2nd Edition, Springer, Berlin. https://doi.org/10.1007/978-3-662-05283-9

Henaish, A., Kharbish, S., Zamzam, S., 2022. Structural controls on drainage pattern using integration of remote sensing and structural data: Insights from Cairo-Suez Province, Egypt. Carpathian J. Earth Environ. Sci. 17 (1), 131–142. https://doi.org/ 10.26471/cjees/2022/017/207.

Hoover, D.B. and Pierce, H.A. (1990): Annotated Bibliography of Gamma-Ray Methods Applied to Gold Exploration.U.S. Geological Survey Report 90-203, pp. 23. https://doi.org/10.3133/ofr90203.

Hoover, D.B., Heran, W.D., Hill, P.L., (1992): The geophysical expression of selected mineral deposit models. U.S. Geological Survey Open-File report 92–557, 129p.

Ibe, S.O. & Nwokeabia, C.N., (2020): International Journal of Advanced Geosciences Application of airborne radiometric method in geologic mapping of Malufashi area and Environs, Northwestern Nigeria. International Journal of Advanced Geosciences, vol.8 (2), P.179-185.

International Atomic Energy Agency (IAEA), 1979: Gamma-ray surveys in uranium exploration. Technical report series 186, Vienna.

Kairu, Edward., (1982): An introduction to remote sensing. GeoJournal. 6. 251-260. 10.1007/BF00210657.

Kamel, M., Youssef, M., Hassan, M., Bagash, F., (2016): Utilization of ETM+Landsat data in geologic mapping of Wadi Ghadir-Gabal Zabara area, Central Eastern Desert, Egypt. Egypt. J. Remote Sens. Space Sci. 19, 343–360.

Lo, B.H., Pitcher, D.H., (1996): A case history on the use of regional aeromagnetic and radiometric data sets for lode gold exploration in Ghana. Annual Meeting Expanded Abstracts, Society of Exploration Geophysicists, 592-595.

Marghany, M., Hashim, M., (2010): Lineament mapping using multispectral remote sensing satellite data. Int. J. Phys. Sci. 5, 1501–1507.

Minty, B.R.S, 1997. Fundamentals of airborne gamma-ray spectrometry. AGSO J. Aust. Geol. Geophys., 17, 39–50.

Moustafa R.A., and Fouda G.H., (1988): Gebel Surf El Dara accommodation zone southwestern part of the Suez rift: M.E.R.C. Ain Shams University, Earth Sc.., Vol. 2, 227-239.

Mwaniki, M.W., Moeller, M.S., Schellmann, G., (2015): A comparison of Landsat 8 (OLI) and Landsat 7 (ETM+) in mapping geology and visualizing lineaments: A case study of central region Kenya. In: The International Archives of the Photogrammetry, Remote Sensing and Spatial Information Sciences. Vol. XL-7/W3, pp. 897–903.

Ramadan, T.M., Abdelsalam, M.G. and Stern, R.J. (2001): Mapping Gold-Bearing Massive Sulfide Deposits in the Neoproterozoic Allaqi Suture, Southeast Egypt with Landsat TM and SIR-C/X SAR Images. Photogrammetric Engineering & Remote Sensing, 67, 491-497.

Ramadan, T.M. and Sultan, S.A. (2004): Integration of Remote Sensing, Geological and Geophysical Data for the Identification of Massive Sulphide Zones at Wadi Al-laqi Area, South Eastern Desert, Egypt. Vol. 18, MERC, Ain Shams University, Cai-ro, 165-174.

Said, R., 1962: Geology of Egypt. Elsevier Publ. Co., Amsterdam and New York, 293–319.

Sanderson, D.C.W., Allyson, J.D., Tyler, A.N., Scott, E.M., (1995): "Environmental applications of airborne gamma ray spectrometry," Application of Uranium Exploration Data and Techniques in Environmental Studies, IAEA-TECDOC-827, IAEA, Vienna, 71-79.

Sanusi, S.O.& Amigun, J.O., (2020): Structural and hydrothermal alteration mapping related to orogenic gold mineralization in part of Kushaka schist belt, North-central Nigeria, using airborne magnetic and gamma-ray spectrometry data. SN Applied Sciences. 2. 10.1007/s42452-020-03435-1.

Sultan, M., Arvidson, R.E. and Sturchio, N.C. (1986): Mapping of Serpentinites in the Eastern Desert of Egypt by Using Landsat Thematic Mapper Data. The Journal of Geology, 14, 995-999.

Takyi-Kyeremeh, K., Wemegah, D.D., Preko, K. and Menyeh, A. (2019): Integrated Geophysical Study of the Subika Gold Deposit in the Sefwi Belt, Ghana. Cogent Geoscience, vol. 5, pp. 1-16.

Wilford, J.R., Bierwirth, P.N., and Craig, M.A., (1997): Application of airborne gamma ray spectrometry in soil/regolith mapping and applied geomorphol-ogy; AGSO J. of Australian Geology and Geophysics, v. 17, No. 2, p. 201-216.

Zoheir, B., Emam, A., Abdel-Wahed, M., Soliman, N., (2019): Multispectral and radar data for the setting of gold mineralization in the South-Eastern desert, Egypt. RemotSens. 11 https://doi.org/10.3390/rs11121450.